



Minerva Access is the Institutional Repository of The University of Melbourne

Author/s:

Marlton, SJP;Liu, C;Bieske, EJ

Title:

Bond dissociation energy of FeCr⁺ determined through threshold photodissociation in a cryogenic ion trap

Date:

2024-01-21

Citation:

Marlton, S. J. P., Liu, C. & Bieske, E. J. (2024). Bond dissociation energy of FeCr⁺ determined through threshold photodissociation in a cryogenic ion trap. *Journal of Chemical Physics*, 160 (3), <https://doi.org/10.1063/5.0188157>.

Persistent Link:


<https://hdl.handle.net/11343/340297>

License:

CC BY

RESEARCH ARTICLE | JANUARY 16 2024

Bond dissociation energy of FeCr^+ determined through threshold photodissociation in a cryogenic ion trap

Samuel J. P. Marltton ; Chang Liu; Evan J. Bieske  



J. Chem. Phys. 160, 034301 (2024)

<https://doi.org/10.1063/5.0188157>




View
Online




Export
Citation

CrossMark



The Journal of Chemical Physics
Special Topic: Algorithms and Software
for Open Quantum System Dynamics
Submit Today



Bond dissociation energy of FeCr^+ determined through threshold photodissociation in a cryogenic ion trap

Cite as: J. Chem. Phys. 160, 034301 (2024); doi: 10.1063/5.0188157

Submitted: 20 November 2023 • Accepted: 20 December 2023 •

Published Online: 16 January 2024



View Online



Export Citation



CrossMark

Samuel J. P. Marlton,  Chang Liu, and Evan J. Bieske^{a)} 

AFFILIATIONS

School of Chemistry, The University of Melbourne, Melbourne, Victoria 3010, Australia

^{a)} Author to whom correspondence should be addressed: evanjb@unimelb.edu.au

ABSTRACT

The bond dissociation energy of FeCr^+ is measured using resonance enhanced photodissociation spectroscopy in a cryogenic ion trap. The onset for $\text{FeCr}^+ \rightarrow \text{Fe} + \text{Cr}^+$ photodissociation occurs well above the lowest $\text{Cr}^+(^6\text{S}, 3\text{d}^5) + \text{Fe}(^5\text{D}, 3\text{d}^6 4\text{s}^2)$ dissociation limit. In contrast, the higher energy $\text{FeCr}^+ \rightarrow \text{Fe}^+ + \text{Cr}$ photodissociation process exhibits an abrupt onset at the energy of the $\text{Cr}(^7\text{S}, 3\text{d}^5 4\text{s}^1) + \text{Fe}^+(^6\text{D}, 3\text{d}^6 4\text{s}^1)$ limit, enabling accurate dissociation energies to be extracted: $D(\text{Fe}-\text{Cr}^+) = 1.655 \pm 0.006$ eV and $D(\text{Fe}^+-\text{Cr}) = 2.791 \pm 0.006$ eV. The measured $D(\text{Fe}-\text{Cr}^+)$ bond energy is 10%–20% larger than predictions from accompanying CAM (Coulomb Attenuated Method)-B3LYP and NEVPT2 and coupled cluster singles, doubles, and perturbative triples electronic structure calculations, which give $D(\text{Fe}-\text{Cr}^+) = 1.48, 1.40,$ and 1.35 eV, respectively. The study emphasizes that an abrupt increase in the photodissociation yield at threshold requires that the molecule possesses a dense manifold of optically accessible, coupled electronic states adjacent to the dissociation asymptote. This condition is not met for the lowest $\text{Cr}^+(^6\text{S}, 3\text{d}^5) + \text{Fe}(^5\text{D}, 3\text{d}^6 4\text{s}^2)$ dissociation limit of FeCr^+ but is satisfied for the higher energy $\text{Cr}(^7\text{S}, 3\text{d}^5 4\text{s}^1) + \text{Fe}^+(^6\text{D}, 3\text{d}^6 4\text{s}^1)$ dissociation limit.

© 2024 Author(s). All article content, except where otherwise noted, is licensed under a Creative Commons Attribution (CC BY) license (<http://creativecommons.org/licenses/by/4.0/>). <https://doi.org/10.1063/5.0188157>

I. INTRODUCTION

The bonding in small transition metal molecules and clusters is a matter of ongoing interest due to the importance of metal–metal bonds in diverse chemical situations. Small metal clusters have electronic properties that can be harnessed in catalysis,¹ serve as model catalysts for gas-phase activation of N_2 and methane,^{2–6} and are key to O_2 sensitivity in enzymes.⁷ The fundamental importance of small transition metal molecules and clusters has motivated numerous computational investigations focusing on their structures, energetics, and reactivity.^{8–10} Transition metal clusters are challenging computational targets with debate over the electronic structures and properties for even small iron and chromium molecules (Cr_2 ,¹¹ Cr_2^+ ,¹² Fe_2 ,^{13,14} and $\text{Fe}_2^{+13–15}$). The molecular bond dissociation energy (BDE) is a measurable quantity for transition metal diatomic molecules that can be used to benchmark various computational approaches, providing a fundamental point of contact between theory and experiment. BDEs have been experimentally determined for

charged metal diatomic molecules using techniques that include collision induced dissociation (CID),^{16,17} velocity map imaging,¹⁸ and resonance enhanced photodissociation (REPD) spectroscopy,¹⁹ and for neutral transition metal diatomic molecules by monitoring the suppression of multiphoton ionization due to predissociation from an excited state.²⁰

In this study, we investigate the FeCr^+ diatomic molecule by measuring its REPD spectrum in a cryogenic ion trap and by conducting corresponding electronic structure calculations. Motivations for studying FeCr^+ include the role $\text{Fe} \cdots \text{Cr}$ bonds play in metal alloys, particularly in stainless steel, and in some inorganic compounds containing covalent $\text{Fe}-\text{Cr}$ bonds featuring remarkably short $\text{Fe} \cdots \text{Cr}$ bonds (< 2 Å) and rich redox chemistry.^{21,22} Despite their importance, there have been few previous experimental or theoretical investigations of Fe_xCr_y^+ clusters. In early studies, Hettich and Freiser reported a low resolution REPD spectrum of the FeCr^+ molecule.²³ BDEs were deduced from the formation onset for the lower energy $\text{Cr}^+ + \text{Fe}$ products with $D(\text{Fe}-\text{Cr}^+) = 50 \pm 7$ kcal/mol

(2.17 ± 0.30 eV) and $D(\text{Fe}^+ - \text{Cr}) = 75 \pm 7$ kcal/mol (3.25 ± 0.30 eV).²³ These experimental bond energies are consistent with computational predictions made by the authors of the work of Gutsev *et al.*, who as part of their extensive study of first-row transition metal diatomic molecules predicted a relatively weak bond [$D(\text{Fe}-\text{Cr}^+) = 2.27$ eV] and a $^2\Delta$ ground state for FeCr^+ .⁹

Under favorable circumstances, REPD spectroscopy is perhaps the most accurate approach for measuring BDEs for charged clusters.^{20,24,25} Ideally, there is an abrupt increase in photofragment signal when the photon energy exceeds the dissociation energy. Photofragment onsets in REPD spectra have been used to ascertain BDEs for several diatomic metal cations, including Ti_2^+ , V_2^+ , Co_2^+ , SmO^+ , and Fe_2^+ ,^{24–26} and also polyatomic transition metal clusters.^{19,24,27} Spain and Morse outlined the following criteria that should be satisfied for the photofragment yield to rise abruptly at the BDE:^{24,28} (1) There is a suitable manifold of optically accessible vibronic states spanning the dissociation limit; (2) dissociation to produce ground state atoms is feasible while preserving good quantum numbers; and (3) the excited molecules can dissociate to ground state atoms without an impeding energy barrier. Photodissociation of transition metal systems is often expedited by dense manifolds of vibronic states that interact through spin-orbit coupling (SOC). When energetically feasible, SOC enables the molecule to couple with the dissociation continuum to produce ground state atoms.

There are many examples of transition metal systems for which the three Spain–Morse conditions are satisfied and where a sharp onset in photofragment yield can be convincingly associated with the BDE.^{24–26} However, some transition metal diatomic molecules lack suitable optically accessible excited states near threshold or do not have a sufficient density of coupled states to provide a pathway to separated atoms. For example, molecules containing transition metal atoms with $(2S+1)S$ ground states (Cr, Mn, Cu, Zn, Mo, Tc, Pd, Ag, Cd, Re, Au, and Hg) have fewer molecular electronic states compared to molecules containing metals with $(2S+1)D$ and $(2S+1)F$ atomic ground states.²⁰ Two instructive examples are Fe_2^+ and Cr_2^+ , both of which undergo photodissociation in the visible spectral range. Fe_2^+ has a high density of optically accessible states spanning the lowest dissociation limit and 750 spin-orbit electronic states correlating with ground state atoms. Thus, the REPD spectrum of Fe_2^+ exhibits a sharp onset for production of Fe^+ photofragments when the photon energy exceeds the BDE (2.529 eV).²⁶ In contrast, for Cr_2^+ the photodissociation onset occurs at 2.13 eV,^{12,29,30} significantly higher than the BDE measured using collision induced dissociation (1.3 eV).¹⁶ The elevated onset for Cr_2^+ photodissociation reflects the absence of suitable optically accessible excited states below 2.13 eV, as subsequently shown through measurements of the Cr_2^+ optical absorption spectrum using cavity ring-down spectroscopy.³⁰

Here, we examine the photodissociation behavior of FeCr^+ as a function of excitation wavelength, finding that it has characteristics of both Cr_2^+ and Fe_2^+ . Notably, formation of Cr^+ photofragments has a gradual onset well above the expected $\text{Fe} + \text{Cr}^+$ dissociation limit, whereas at higher photon energy there is an abrupt onset for Fe^+ photofragments appearing at the lowest energy $\text{Fe}^+ + \text{Cr}$ dissociation limit where there is a far higher density of electronic states. We rationalize the photodissociation behavior with the aid of calculated potential energy curves describing the ground and excited

states of FeCr^+ . On the basis of the current work, we believe that the BDEs reported by Hettich and Freiser,²³ and calculated in the work of Gutsev *et al.*,⁹ substantially overestimate the actual value.

II. METHODS

A. Experimental

The experimental apparatus has been described previously.^{26,31} It consists of a laser ablation ion source followed by a drift tube ion mobility spectrometer (IMS), a differentially pumped hexapole, a quadrupole mass filter (QMF), an octupole ion guide, a cryogenically cooled quadrupole ion trap (QIT), and a time-of-flight (ToF) mass spectrometer. Briefly, FeCr^+ clusters were generated by ablating a rotating disk of tool steel with the focused output of a frequency-doubled pulsed Nd:YAG laser ($\lambda = 532$ nm, 3 mJ/pulse, 100 Hz). Following their creation, the ions were propelled by an electric field (10 V cm^{-1}) through a drift region containing He buffer gas ($P \approx 2$ Torr). At the end of the drift region, the ion bunch was compressed radially using an RF ion funnel and passed through a 1 mm orifice into a differentially pumped region containing an RF hexapole ($P \approx 5 \times 10^{-5}$ Torr). The ions were accumulated in the hexapole for 500 ms, after which the potential of an electrostatic lens at the hexapole exit was dropped to allow the ions to exit the hexapole and enter the quadrupole mass filter (QMF). The QMF was set to select $^{56}\text{Fe}^{52}\text{Cr}^+$ ions, which were then transmitted by an octupole ion guide into a three-dimensional quadrupole ion trap (QIT) mounted on a cryohead ($T \approx 10$ K), where they were collisionally cooled by He gas injected through a pulsed valve into the trap at 2 Hz. The ions were allowed to cool in the QIT for 100 ms and then in alternate trapping cycles they were exposed to six light pulses from a tunable optical parametric oscillator (OPO, EKSPLA NT342B, 6 ns pulse width, bandwidth ≈ 4 cm^{-1} , pulse energy ≈ 10 mJ cm^{-2} pulse^{-1} , repetition rate 20 Hz). Admission of the light pulses to the ion trap was controlled using a mechanical shutter. Approximately 30 ms after the last light pulse, the ions were ejected from the QIT into a linear time-of-flight mass spectrometer (ToF MS). REPD spectra for FeCr^+ were recorded by monitoring Cr^+ and Fe^+ photoproducts (laser-on minus laser-off signal) as a function of OPO wavelength. Because the ions were trapped for >30 ms after exposure to the last light pulse, the method should be sensitive to slow photodissociation processes so that the measured thresholds should not be influenced by kinetic effects. It should be noted that the FeCr^+ ions had ample time (50–500 ms) to relax electronically, vibrationally, and rotationally before they were exposed to light from the tunable OPO. It is also relevant to note that reducing the light intensity or number of light pulses did not significantly affect the appearance of the FeCr^+ REPD spectra.

B. Theoretical

Potential energy curves (PECs) for FeCr^+ were calculated using the ORCA/5.0.2 program package.^{32,33} All calculations employed the segmented all-electron relativistically contracted (SARC) Coulomb fitting basis set,^{34,35} and the relativistic second-order Douglas–Kroll–Hess (DKH) Hamiltonian.³⁶ Unrestricted coupled cluster singles, doubles, and perturbative triples [CCSD(T)] calculations were undertaken using the DKH-def2-TZVP basis set.^{34,35} N -electron valence second-order perturbation

theory (NEVPT2)³⁷ calculations were carried out using complete active space self-consistent field (CASSCF) wavefunctions³⁸ and the DKH-def2-SVP basis set.^{34,35} The CASSCF active space, referred to as CASSCF(13,12), was composed of the five 3d and 4s orbitals for Fe and Cr, as shown in Fig. 2. The CASSCF(13,12) reference included equal state averaging of the ten doublet, quartet, sextet, octet, and decet potential energy curves that correlate with $\text{Cr}^+(^6\text{S}, 3d^5) + \text{Fe}(^5\text{D}, 3d^6 4s^2)$ and $\text{Cr}(^7\text{S}, 3d^5 4s^1) + \text{Fe}^+(^6\text{D}, 3d^6 4s^1)$ atoms. Spin-orbit coupling (SOC) was included by quasi-degenerate perturbation theory using NEVPT2 energies.³⁹ Hereon, this approach is referred to as SOC+NEVPT2. States correlating with $\text{Cr}^+(^6\text{S}, 3d^5) + \text{Fe}(^5\text{F}, 3d^7 4s^1)$ could not be calculated using this approach, apparently because the CASSCF reference significantly overestimates their energies. Density functional theory (DFT) calculations were undertaken employing the range separated CAM (Coulomb Attenuated Method)-B3LYP hybrid functional⁴⁰ with the DKH-def2-QZVPP basis set.

The vibrational zero-point energy for the ground state of FeCr^+ was determined by fitting the calculated potential energy points with a cubic spline and numerically solving the ro-vibrational Schrödinger equation with the VibRot program in MOLCAS.⁴¹ The difference in Cr and Fe ionization potentials (ΔIP) was calculated with NEVPT2 at a $\text{Fe} \cdots \text{Cr}$ separation of 20 Å, and with CCSD(T) and CAM-B3LYP by separately calculating $\text{IP}(\text{Fe})$ and $\text{IP}(\text{Cr})$. The calculated $D(\text{Fe}^+-\text{Cr})$ values are the sum of the calculated ΔIP and $D(\text{Fe}-\text{Cr}^+)$ values (see Fig. 1).

III. RESULTS

A. Potential energy curves for FeCr^+

Details for the five lowest energy dissociation limits for FeCr^+ are compiled in Table I. Combining the two atoms gives rise to a series of molecular states whose nature can be determined from the Wigner–Witmer rules.⁴² For example, the lowest energy dissociation limit, $\text{Cr}^+(^6\text{S}, 3d^5) + \text{Fe}(^5\text{D}, 3d^6 4s^2)$, gives rise to a Σ^+ state, a pair of doubly degenerate Π states, and a pair of doubly degenerate Δ states, each of which can have doublet, quartet, sextet, octet, or decet multiplicity ($2S + 1$). This yields a total of 25 molecular (Λ, S) electronic states. These (Λ, S) states are split by spin-orbit coupling (SOC), giving 75 molecular SOC states. The energies and number of molecular electronic states correlating with each of the lowest five dissociation limits of FeCr^+ are listed in Table I. For comparison, the lowest dissociation limit of Cr_2^+ correlates with 42 SOC states, while the lowest dissociation limit of Fe_2^+ correlates with 750 SOC states.

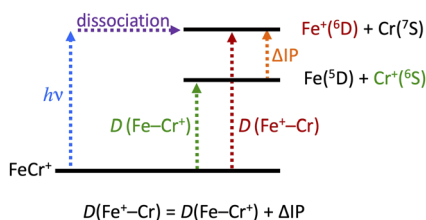


FIG. 1. Relationship between energies of the FeCr^+ diatomic molecule and the $\text{Cr}^+(^6\text{S}, 3d^5) + \text{Fe}(^5\text{D}, 3d^6 4s^2)$ and $\text{Cr}(^7\text{S}, 3d^5 4s^1) + \text{Fe}^+(^6\text{D}, 3d^6 4s^1)$ dissociation limits.

TABLE I. The five lowest dissociation limits of FeCr^+ along with the number of molecular states that correlate with each limit ignoring SOC (Λ, S) and including SOC. The energies for each limit are given relative to the lowest energy limit as determined from NIST data.^{43–45}

Dissociation limit	Energy above		
	GS atoms (cm^{-1})	(Λ, S) states	SOC states
$\text{Cr}^+(^6\text{S}) + \text{Fe}(^5\text{D})$	0	25	75
$\text{Cr}^+(^6\text{S}) + \text{Fe}(^5\text{F})$	6 928	35	105
$\text{Cr}(^7\text{S}) + \text{Fe}^+(^6\text{D})$	9 161	30	105
$\text{Cr}(^7\text{S}) + \text{Fe}^+(^4\text{F})$	11 033	35	98
$\text{Cr}^+(^6\text{D}) + \text{Fe}(^5\text{D})$	11 962	125	375

PECs for SOC states correlating with the $\text{Cr}^+(^6\text{S}) + \text{Fe}(^5\text{D})$ and $\text{Cr}(^7\text{S}) + \text{Fe}^+(^6\text{D})$ dissociation limits are shown in Fig. 2(a). The PECs were calculated using the SOC+NEVPT2 method (gray dots) and CCSD(T) (solid lines). The solid black curve in Fig. 2(a) corresponds to the CCSD(T) ground state for FeCr^+ . Both the CCSD(T) and SOC+NEVPT2 calculations predict a $^2\Sigma^+$ ground state for FeCr^+ with the dominant electronic configuration shown in Fig. 2(b). Reliably assigning the ground state is difficult because six different SOC states are predicted to lie within 400 cm^{-1} of the ground state. Previously, the authors of the work of Gustev *et al.* proposed a $^2\Delta$ ground state based on DFT calculations at the BPW91/6-311+G* level.⁹ However, some caution is warranted as BPW91/6-311+G* calculations incorrectly predict a $^2\Sigma^+$ ground state for Cr_2^+ instead of $^{12}\Sigma^{+12}$ and a $^7\Delta_u$ ground state for Fe_2 rather than $^9\Sigma_g^-$.^{13,14}

The PECs correlating with the second lowest dissociation limit [$\text{Cr}^+(^6\text{S}) + \text{Fe}(^5\text{F})$] could not be reliably calculated with NEVPT2 or CCSD(T), presumably because their energies are overestimated by the CASSCF reference relative to other low-lying states. The green dashed curve in Fig. 2(a) corresponds to a hypothetical potential energy curve correlating with $\text{Cr}^+(^6\text{S}) + \text{Fe}(^5\text{F})$ atom that has been included to help visualize the states correlating with this asymptote. As explained below, PECs emanating from this dissociation limit should be relatively shallow. Calculated potential energy curves associated with the next higher limit [$\text{Cr}(^7\text{S}) + \text{Fe}^+(^6\text{D})$], the lowest energy limit giving Fe^+ fragments, are shown in Fig. 2(a). The solid red curve in Fig. 2(a) corresponds to the lowest dodecet state calculated using CCSD(T).

The shallow nature of PECs correlating with the $\text{Cr}^+(^6\text{S}, 3d^5) + \text{Fe}(^5\text{F}, 3d^7 4s^1)$ and $\text{Cr}(^7\text{S}, 3d^5 4s^1) + \text{Fe}^+(^6\text{D}, 3d^6 4s^1)$ dissociation limits can be rationalized by considering the occupation of the σ bonding and σ^* antibonding orbitals that influence the bonding for first-row transition metal dimers.^{24,46,47} Molecular orbitals generated from atomic 3d orbitals are of mostly nonbonding character. For FeCr^+ , the bonding σ molecular orbital is derived mainly from the 4s atomic orbital of Fe, while the antibonding σ^* molecular orbital is principally generated from the 4s atomic orbital of Cr. Molecular states of FeCr^+ correlating with ground state atoms [$\text{Cr}^+(^6\text{S}, 3d^5) + \text{Fe}(^5\text{D}, 3d^6 4s^2)$] have a doubly occupied σ^2 bonding orbital, whereas states correlating with the higher energy dissociation asymptotes [$\text{Cr}^+(^6\text{S}, 3d^5) + \text{Fe}(^5\text{F}, 3d^7 4s^1)$ and $\text{Cr}(^7\text{S}, 3d^5 4s^1) + \text{Fe}^+(^6\text{D}, 3d^6 4s^1)$] have a singly occupied σ^1

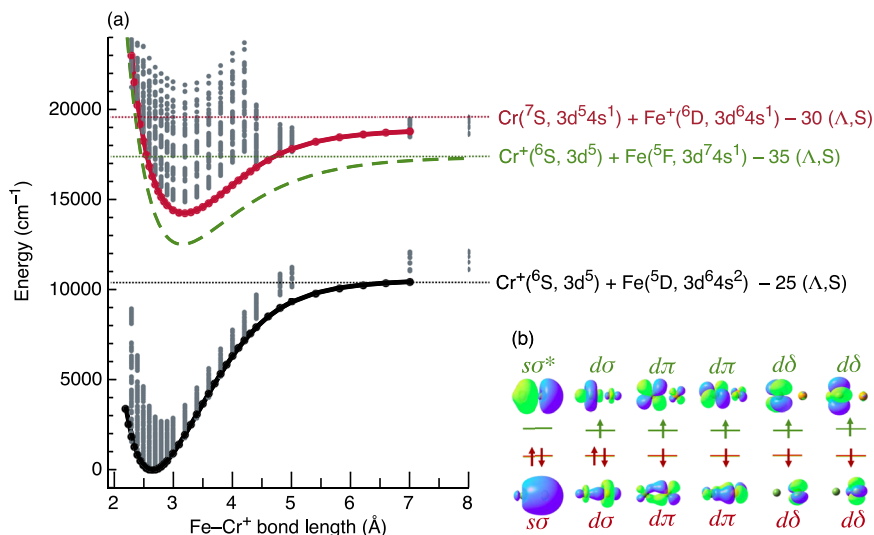


FIG. 2. (a) Potential energy curves for SOC states of FeCr^+ correlating with ground state atoms $\text{Cr}^+(\text{}^6\text{S}, 3d^5) + \text{Fe}(\text{}^5\text{D}, 3d^6 4s^2)$ and with the excited $\text{Cr}(\text{}^7\text{S}, 3d^5 4s^1) + \text{Fe}(\text{}^6\text{D}, 3d^6 4s^1)$ limit. Points on PECs calculated using SOC+NEVPT2 are shown as gray dots. The PECs for the lowest energy doublet (black trace) and lowest energy dodeclet (red trace) calculated using CCSD(T) are also shown. The green dashed line shows a hypothetical PEC correlating with $\text{Cr}^+(\text{}^6\text{S}, 3d^5) + \text{Fe}(\text{}^5\text{F}, 3d^7 4s^1)$ atoms. The numbers of (Λ , S) molecular electronic states generated from these atomic fragments without considering spin-orbit coupling are indicated. (b) Active space orbitals used for CASSCF and NEVPT2 calculations. The electronic configuration shown is the dominant configuration for the lowest ${}^2\Sigma^+$ electronic state.

bonding orbital, resulting in shallower wells and longer bonds than states with a $s\sigma^2$ configuration.^{24,46,47}

B. Photodissociation and bond energetics

Exposing the FeCr^+ ions to visible light in the QIT produced Cr^+ and Fe^+ photofragments with a branching ratio that depended on wavelength. The effect of light is apparent in Fig. 3, which shows the difference between ToF mass spectra obtained with the dissociation laser on and dissociation laser off. Exposure to $22\,472\text{ cm}^{-1}$ photons yields significantly more ${}^{52}\text{Cr}^+$ than ${}^{56}\text{Fe}^+$; however, the ${}^{52}\text{Cr}^+$ and ${}^{56}\text{Fe}^+$ photoproduct signals are comparable if the photon energy is increased by 102 cm^{-1} to $22\,574\text{ cm}^{-1}$ [the photon energies for dissociation are indicated in REPD spectrum shown in Fig. 4(b)]. As discussed below, this change in photoproduct branching ratio occurs when the photon energy exceeds the lowest $\text{Fe}^+ + \text{Cr}$ dissociation limit. The minor m/z 54 peak in the mass spectrum is due to ${}^{54}\text{Fe}^+$ photofragments from ${}^{54}\text{Fe}_2^+$, which is isobaric with ${}^{56}\text{Fe}{}^{52}\text{Cr}^+$.

The REPD spectrum of FeCr^+ measured over the 410–690 nm range is shown in Fig. 4. As the photon energy is increased, the Cr^+ signal (green trace) exhibits a gradual onset at $\approx 17\,000\text{ cm}^{-1}$, consistent with the previous measurements by Hettich and Freiser.²³ At $22\,510\text{ cm}^{-1}$, there is an abrupt increase in the Fe^+ photoproduct signal coinciding with a decrease in the Cr^+ photoproduct signal [Fig. 4(b)]. This steep rise in Fe^+ photofragment yield resembles sharp photodissociation onsets observed for other transition metal dimers including Ti_2^+ , V_2^+ , Co_2^+ , and Fe_2^+ at their dissociation limits.^{24–26} To investigate whether Fe^+ product ions were formed by one-photon dissociation, power dependence measurements were conducted with light at $22\,568\text{ cm}^{-1}$,

$\approx 58\text{ cm}^{-1}$ above the Fe^+ REPD onset. As shown in Fig. 5, both ${}^{56}\text{Fe}^+$ and ${}^{52}\text{Cr}^+$ photoproduct yields exhibit a linear dependence on laser power, consistent with single photon dissociation processes.

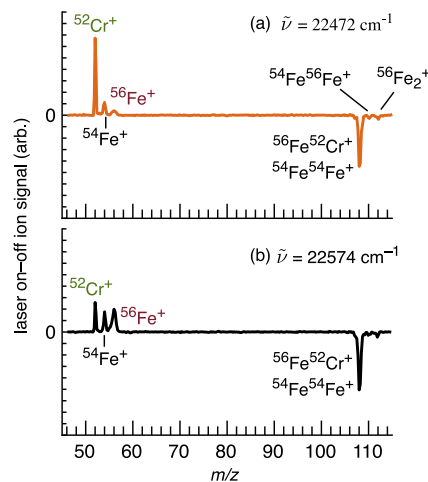


FIG. 3. Light-on minus light-off photodissociation mass spectra for ${}^{56}\text{Fe}{}^{52}\text{Cr}^+$ with OPO light tuned to (a) $22\,472\text{ cm}^{-1}$ (orange trace) and (b) $22\,574\text{ cm}^{-1}$ (lower, black trace). The photoexcitation energies are indicated in the REPD spectrum shown Fig. 4(b). Isobaric ${}^{54}\text{Fe}_2^+$ ions yield ${}^{54}\text{Fe}^+$ photoproducts that are distinguishable from ${}^{56}\text{Fe}^+$ and ${}^{52}\text{Cr}^+$ photoproducts from ${}^{56}\text{Fe}{}^{52}\text{Cr}^+$. ${}^{56}\text{Fe}^+$ photofragment ions are also formed from small populations of ${}^{54}\text{Fe}{}^{56}\text{Fe}^+$ and ${}^{56}\text{Fe}_2^+$ ions present in the QIT.

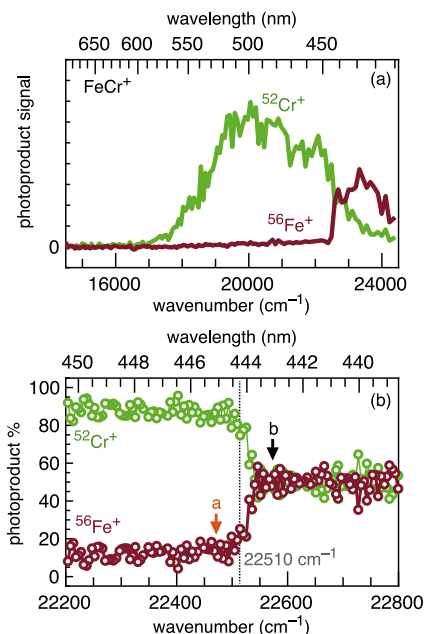


FIG. 4. (a) REPD spectrum of FeCr^+ in the visible region following the photoproduct signal of Cr^+ (green trace) and Fe^+ (red trace). (b) Relative yields of Cr^+ (green circles) and Fe^+ (red circles) photoproduct ions in the vicinity of the Fe^+ REPD threshold. Sub-threshold $^{56}\text{Fe}^+$ ions are photofragments from background $^{54}\text{Fe}^{56}\text{Fe}^+$ and $^{56}\text{Fe}^{2+}$ ions present in the QIT. Arrows indicate the excitation energies for the photodissociation mass spectra shown in Figs. 3(a) and 3(b).

Assuming that the energy for sharp onset for Fe^+ photofragments corresponds to the $\text{Cr}({}^7\text{S}, 3d^5 4s^1) + \text{Fe}^+({}^6\text{D}, 3d^6 4s^1)$ dissociation threshold implies $D(\text{Fe}^+-\text{Cr}) = 22\,510 \pm 50 \text{ cm}^{-1}$ ($2.791 \pm 0.006 \text{ eV}$) and $D(\text{Fe}-\text{Cr}^+) = D(\text{Fe}^+-\text{Cr}) - \Delta\text{IP} = 13\,350 \pm 50 \text{ cm}^{-1}$ ($1.655 \pm 0.006 \text{ eV}$) (using $\Delta\text{IP} = 1.1359 \text{ eV} = 9161 \text{ cm}^{-1}$, Ref. 45). As shown in Fig. 4(a), the onset for Cr^+ formation occurs at $\approx 17\,000 \text{ cm}^{-1}$, 4000 cm^{-1} above the actual dissociation energy, $D(\text{Fe}-\text{Cr}^+)$. The absence of Cr^+ photofragments for photon energies near the $\text{Cr}^+({}^6\text{S}) + \text{Fe}({}^5\text{D})$ dissociation limit is presumably because there are no optically accessible states in the vicinity. Generally, in order to produce photofragments associated with the lowest dissociation limit, it is necessary that PECs correlating with a higher dissociation limit dip below the lowest dissociation asymptote. As discussed above, PECs correlating with the excited $\text{Cr}^+({}^6\text{S}, 3d^5) + \text{Fe}({}^5\text{F}, 3d^7 4s^1)$ and $\text{Cr}({}^7\text{S}, 3d^5 4s^1) + \text{Fe}^+({}^6\text{D}, 3d^6 4s^1)$ limits are likely to be shallow with minima lying above the $\text{Cr}^+({}^6\text{S}) + \text{Fe}({}^5\text{D})$ dissociation limit. Furthermore, because the equilibrium bond lengths associated with these molecular states will exceed the bond length for the electronic ground state, the first few vibronic transitions from the ground state should have small Franck–Condon factors. This is consistent with the gradual onset for formation of Cr^+ photoproducts. As a consequence, the earlier bond dissociation energy reported by Hettich and Freiser [$D(\text{Fe}-\text{Cr}^+) = 2.17 \pm 0.30 \text{ eV}$], based on the onset for Cr^+ photoproducts,²³ overestimates the actual value by 0.52 eV .

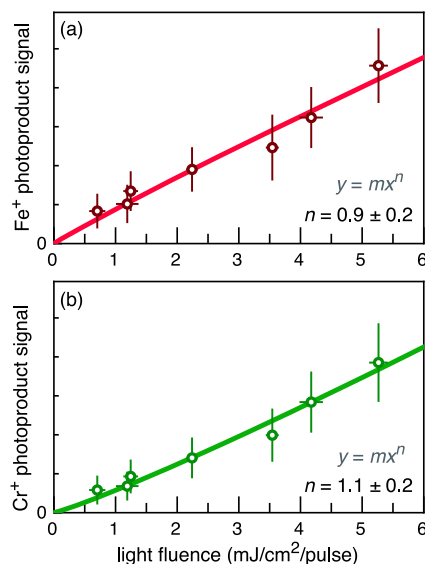


FIG. 5. Light fluence dependence for photodissociation of FeCr^+ to yield (a) Fe^+ photoproducts, and (b) Cr^+ photoproducts using $22\,568 \text{ cm}^{-1}$ (2.798 eV) photons. Each ion packet was exposed to six laser pulses. Data point error bars correspond to $\pm 1\sigma$ relative errors. The reported uncertainty for n is $\pm 2\sigma$.

The situation is different for photodissociation to produce Fe^+ fragments. At the $\text{Cr}({}^7\text{S}) + \text{Fe}^+({}^6\text{D})$ dissociation limit, there is a high density of optically accessible excited vibronic states as evidenced by the steady production of Cr^+ photofragments across the $18\,000\text{--}24\,000 \text{ cm}^{-1}$ range (Fig. 4). Moreover, the SOC+NEVPT2 calculations predict a high density of excited electronic states spanning the $\text{Cr}({}^7\text{S}) + \text{Fe}^+({}^6\text{D})$ dissociation limit [see Fig. 2(a)]. Evidently, the excited states are strongly coupled so that dissociation to give $\text{Cr}({}^7\text{S}) + \text{Fe}^+({}^6\text{D})$ products occurs right at the dissociation limit.

The new experimental BDEs for FeCr^+ allow us to make comparisons with similar systems and to assess the performance of various computational approaches. Previous BPW91/6-311+G* calculations from the work of Gustev *et al.* predicted $D(\text{Fe}-\text{Cr}^+)$

TABLE II. Measured and calculated values for $D(\text{Fe}-\text{Cr}^+)$ and $D(\text{Fe}^+-\text{Cr})$ for FeCr^+ obtained in this work, through previous REPD measurements (Ref. 23), and from BPW91/6-311+G* calculations (Ref. 9).

	$D(\text{Fe}-\text{Cr}^+)$ (eV)	$D(\text{Fe}^+-\text{Cr})$ (eV)	ΔIP (eV)
REPD ^a	1.655(6)	2.791(6)	1.136 ^b
REPD ^c	2.17(30)	3.25(30)	1.136 ^b
BPW91 ^d	2.27		
CAM-B3LYP ^a	1.478	2.527	1.049
NEVPT2 ^a	1.401	2.328	0.927
CCSD(T) ^a	1.346	2.381	1.035

^aThis work.

^bReferences 43–45.

^cReference 23.

^dReference 9.

= 2.27 eV,⁹ exceeding the experimental value by 0.68 eV. Calculated $D(\text{Fe}-\text{Cr}^+)$ values determined in the current study are closer to the experimental value but are too low by 0.18 eV (CAM-B3LYP), 0.25 eV (NEVPT2), and 0.31 eV [CCSD(T)] (see Table II). Compared to related systems, the bond for FeCr^+ [$D(\text{Fe}-\text{Cr}^+) = 1.655$ eV, $r_e = 2.7$ Å] is stronger than the Cr_2^+ bond [$D(\text{Cr}-\text{Cr}^+) = 1.30$ eV, $r_e = 2.9$ Å]^{12,16} but much weaker than the Fe_2^+ bond [$D(\text{Fe}-\text{Fe}^+) = 2.529$ eV, $r_e = 2.1$ Å].^{13,26}

IV. CONCLUSIONS

We have measured the REPD spectrum of the iron chromium diatomic cation FeCr^+ in a cryogenic ion trap by monitoring the production of Cr^+ and Fe^+ photofragments as a function of photon energy. The lack of optically active excited states near the Cr^+ (^6S) + Fe^+ (^5D) dissociation limit means that there is a gradual onset for Cr^+ photofragments at photon energies well above the limit. On the other hand, a sharp onset for Fe^+ photoproducts at higher photon energy can be plausibly associated with the Cr^+ (^7S) + Fe^+ (^6D) dissociation limit. From the Fe^+ onset energy, one can derive accurate BDE values [$D(\text{Fe}-\text{Cr}^+) = 1.655 \pm 0.006$ eV and $D(\text{Fe}^+-\text{Cr}) = 2.791 \pm 0.006$ eV], around 0.5 eV lower than previously reported experimental BDEs.²³ The new experimental BDEs for FeCr^+ supplement a growing list of BDEs for transition metal diatomic molecules measured with greater than chemical accuracy (0.04 eV),^{20,26} providing benchmark data for different quantum chemical approaches. Ideally, in the future the BDE and ionization potential of neutral FeCr will be measured, allowing the consistency of neutral and cation BDEs to be checked through the thermochemical cycle: $D_0(\text{FeCr}) + \text{IP}(\text{Cr}) = D_0(\text{FeCr}^+) + \text{IP}(\text{FeCr})$.²⁰

Finally, we note that the situation for FeCr^+ , with a gradual increase in Cr^+ production and abrupt onset for Fe^+ production, may apply to other MCr^+ cations for which $\text{IP}(\text{M}) > \text{IP}(\text{Cr})$. This provides hope that BDEs can be measured for systems such as CrCo^+ and CrNi^+ by monitoring thresholds for production of Co^+ or Ni^+ photofragments rather than Cr^+ . More generally, monitoring the onsets for photofragmentation into higher energy channels may help ascertain BDEs for an extended range of metal dimers including molecules containing metal atoms with $\text{S}^{(2S+1)}$ ground states (Cr, Mn, Cu, Zn, Mo, Tc, Pd, Ag, Cd, Re, Au, and Hg), which are difficult targets for threshold photodissociation measurements because the ground state atoms correlate with relatively few molecular electronic states.²⁰ Encouragingly, BDEs have recently been measured for the neutral CrN , CuN , and AuB molecules by observing the suppression of multiphoton ionization at photon energies that correspond to dissociation to atomic fragments in their excited states.⁴⁸ For these systems, as for FeCr^+ , there are few optically accessible, coupled states in the vicinity of the lowest dissociation limit but a conveniently large density of states adjacent to limits associated with separated atoms in excited electronic states.

ACKNOWLEDGMENTS

This research was supported under the Australian Research Council's Discovery Project funding scheme (Project Nos. DP150101427 and DP160100474). The authors thank Richard Mathys from the Science Faculty Workshop for his valuable

contributions to the design and construction of the apparatus used in this study.

AUTHOR DECLARATIONS

Conflict of Interest

The authors have no conflicts to disclose.

Author Contributions

Samuel J. P. Marlton: Conceptualization (equal); Formal analysis (equal); Investigation (equal); Methodology (equal); Writing – original draft (lead); Writing – review & editing (equal). **Chang Liu:** Investigation (equal); Writing – review & editing (supporting). **Evan J. Bieske:** Conceptualization (equal); Funding acquisition (lead); Investigation (supporting); Methodology (equal); Writing – review & editing (equal).

DATA AVAILABILITY

The data that support the findings of this study are available from the corresponding author upon reasonable request.

REFERENCES

- I. G. Powers and C. Uyeda, *ACS Catal.* **7**, 936 (2017).
- A. Straßner, C. Wiehn, M. P. Klein, D. V. Fries, S. Dillinger, J. Mohrbach, M. H. Proscenc, P. Armentrout, and G. Niedner-Schatteburg, *J. Chem. Phys.* **155**, 244305 (2021).
- M. P. Klein, A. A. Ehrhard, M. E. Huber, A. Straßner, D. V. Fries, S. Dillinger, J. Mohrbach, and G. Niedner-Schatteburg, *J. Chem. Phys.* **156**, 014302 (2022).
- A. A. Ehrhard, M. P. Klein, J. Mohrbach, S. Dillinger, and G. Niedner-Schatteburg, *J. Chem. Phys.* **156**, 054308 (2022).
- Y. Y. Wang, X.-L. Ding, Z.-W. Ji, X.-M. Huang, and W. Li, *ChemPhysChem* **24**, e202200952 (2023).
- J. Roithová and J. M. Bakker, *Mass Spectrom. Rev.* **41**, 513 (2022).
- P. A. Lindahl, *J. Inorg. Biochem.* **106**, 172 (2012).
- S. R. Langhoff and C. W. Bauschlicher, Jr., *Annu. Rev. Phys. Chem.* **39**, 181 (1988).
- G. Gutsev, M. Mochena, P. Jena, C. Bauschlicher, Jr., and H. Partridge III, *J. Chem. Phys.* **121**, 6785 (2004).
- N. E. Schultz, Y. Zhao, and D. G. Truhlar, *J. Phys. Chem. A* **109**, 4388 (2005).
- H. R. Larsson, H. Zhai, C. J. Umrigar, and G. K.-L. Chan, *J. Am. Chem. Soc.* **144**, 15932 (2022).
- K. Egashira, Y. Yamada, Y. Kita, and M. Tachikawa, *J. Chem. Phys.* **142**, 054309 (2015).
- C. E. Hoyer, G. L. Manni, D. G. Truhlar, and L. Gagliardi, *J. Chem. Phys.* **141**, 204309 (2014).
- A. Kalamos, *J. Chem. Phys.* **142**, 244304 (2015).
- V. Zamudio-Bayer, K. Hirsch, A. Langenberg, A. Ławicki, A. Terasaki, B. V. Issendorff, and J. Lau, *J. Chem. Phys.* **143**, 244318 (2015).
- C.-X. Su, D. A. Hales, and P. Armentrout, *Chem. Phys. Lett.* **201**, 199 (1993).
- S. Loh, D. A. Hales, L. Lian, and P. B. Armentrout, *J. Chem. Phys.* **90**, 5466 (1989).
- M. D. Johnston, S. P. Lockwood, and R. B. Metz, *J. Chem. Phys.* **148**, 214308 (2018).
- Z. Fu, L. M. Russon, M. D. Morse, and P. Armentrout, *Int. J. Mass Spectrom.* **204**, 143 (2001).
- M. D. Morse, *Acc. Chem. Res.* **52**, 119 (2018).

- ²¹P. A. Rudd, S. Liu, N. Planas, E. Bill, L. Gagliardi, and C. C. Lu, *Angew. Chem., Int. Ed.* **52**, 4449 (2013).
- ²²L. J. Clouston, R. B. Siedschlag, P. A. Rudd, N. Planas, S. Hu, A. D. Miller, L. Gagliardi, and C. C. Lu, *J. Am. Chem. Soc.* **135**, 13142 (2013).
- ²³R. Hettich and B. Freiser, *J. Am. Chem. Soc.* **109**, 3537 (1987).
- ²⁴L. M. Russon, S. A. Heidecke, M. K. Birke, J. Conceicao, M. D. Morse, and P. B. Armentrout, *J. Chem. Phys.* **100**, 4747 (1994).
- ²⁵A. Lachowicz, E. H. Perez, N. S. Shuman, S. G. Ard, A. A. Viggiano, P. B. Armentrout, J. J. Goings, P. Sharma, X. Li, and M. A. Johnson, *J. Chem. Phys.* **155**, 174303 (2021).
- ²⁶S. J. P. Marlton, C. Liu, P. Watkins, J. T. Buntine, and E. J. Bieske, *J. Chem. Phys.* **159**, 024302 (2023).
- ²⁷T. Majima, K. Tono, A. Terasaki, Y. Kawazoe, and T. Kondow, *Eur. Phys. J. D* **43**, 23 (2007).
- ²⁸E. M. Spain and M. D. Morse, *J. Phys. Chem.* **96**, 2479 (1992).
- ²⁹D. Lessen, R. Asher, and P. Brucat, *Chem. Phys. Lett.* **182**, 412 (1991).
- ³⁰K. Egashira and A. Terasaki, *Chem. Phys. Lett.* **635**, 13 (2015).
- ³¹J. T. Buntine, E. Carrascosa, J. N. Bull, U. Jacovella, M. I. Cotter, P. Watkins, C. Liu, M. S. Scholz, B. D. Adamson, S. J. P. Marlton, and E. J. Bieske, *Rev. Sci. Instrum.* **93**, 043201 (2022).
- ³²F. Neese, *Wiley Interdiscip. Rev.: Comput. Mol. Sci.* **2**, 73 (2012).
- ³³F. Neese, *Wiley Interdiscip. Rev.: Comput. Mol. Sci.* **12**, e1606 (2022).
- ³⁴F. Weigend and R. Ahlrichs, *Phys. Chem. Chem. Phys.* **7**, 3297 (2005).
- ³⁵D. A. Pantazis, X.-Y. Chen, C. R. Landis, and F. Neese, *J. Chem. Theory Comput.* **4**, 908 (2008).
- ³⁶A. Wolf, M. Reiher, and B. A. Hess, *J. Chem. Phys.* **117**, 9215 (2002).
- ³⁷C. Angeli, R. Cimraglia, S. Evangelisti, T. Leininger, and J.-P. Malrieu, *J. Chem. Phys.* **114**, 10252 (2001).
- ³⁸B. O. Roos, P. R. Taylor, and P. E. Sigbahn, *Chem. Phys.* **48**, 157 (1980).
- ³⁹M. Sundararajan, D. Ganyushin, S. Ye, and F. Neese, *Dalton Trans.* **2009**, 6021.
- ⁴⁰T. Yanai, D. P. Tew, and N. C. Handy, *Chem. Phys. Lett.* **393**, 51 (2004).
- ⁴¹I. Fdez Galván, M. Vacher, A. Alavi, C. Angeli, F. Aquilante, J. Autschbach, J. J. Bao, S. I. Bokarev, N. A. Bogdanov, R. K. Carlson *et al.*, *J. Chem. Theory Comput.* **15**, 5925 (2019).
- ⁴²G. Herzberg, *Molecular Spectra and Molecular Structure* (Read Books Ltd., 2013), Vol. 1.
- ⁴³G. Nave, S. Johansson, R. C. M. Learner, A. P. Thorne, and J. W. Brault, *Astrophys. J., Suppl. Ser.* **94**, 221 (1994).
- ⁴⁴S. Johansson, *Phys. Scr.* **18**, 217 (1978).
- ⁴⁵S. G. Lias, J. E. Bartmess, J. F. Liebman, J. L. Holmes, R. D. Levin, and W. G. Mallard, "Ion energetics data," *NIST Chemistry WebBook, NIST Standard Reference Database No. 69*, edited by P. J. Linstrom and W. G. Mallard (National Institute of Standards and Technology, 2024).
- ⁴⁶P. Armentrout and J. Simons, *J. Am. Chem. Soc.* **114**, 8627 (1992).
- ⁴⁷T. H. Upton and W. A. Goddard III, *J. Am. Chem. Soc.* **100**, 5659 (1978).
- ⁴⁸D. M. Merriles and M. D. Morse, *J. Phys. Chem. Lett.* **14**, 7361 (2023).